The effect of interactions between failure mechanisms on the reliability of flood defenses

Pol, Johannes C.; Kindermann, Paulina; van der Krogt, Mark G.; van Bergeijk, Vera M.; Remmerswaal, Guido; Kanning, Willem; Jonkman, Sebastiaan N.; Kok, Matthijs

DOI
10.1016/j.ress.2022.108987

Publication date
2023

Document Version
Final published version

Published in
Reliability Engineering & System Safety

Citation (APA)
Pol, J. C., Kindermann, P., van der Krogt, M. G., van Bergeijk, V. M., Remmerswaal, G., Kanning, W., Jonkman, S. N., & Kok, M. (2023). The effect of interactions between failure mechanisms on the reliability of flood defenses. *Reliability Engineering & System Safety*, *231*, Article 108987. https://doi.org/10.1016/j.ress.2022.108987

Reliability Engineering and System Safety 231 (2023) 108987

Contents lists available at ScienceDirect

Reliability Engineering and System Safety

journal homepage: www.elsevier.com/locate/ress

The effect of interactions between failure mechanisms on the reliability of flood defenses

Johannes C. Pol [a,b,*], Paulina Kindermann [b], Mark G. van der Krogt [a,c], Vera M. van Bergeijk [d], Guido Remmerswaal [e,c], Willem Kanning [a,c], Sebastiaan N. Jonkman [a], Matthijs Kok [a,b]

[a] Department of Hydraulic Engineering, Delft University of Technology, Delft, Netherlands
[b] HKV, Lelystad, Netherlands
[c] Unit Geo-engineering, Deltares, Delft, Netherlands
[d] Department of Marine and Fluvial Systems, University of Twente, Enschede, Netherlands
[e] Department of Geo-engineering, Delft University of Technology, Delft, Netherlands

ARTICLE INFO

Keywords:
Reliability
Interaction
Failure mechanisms
Flood defenses
Slope instability
Backward erosion piping

ABSTRACT

Structural reliability analysis often considers failure mechanisms as correlated but non-interacting processes. Interacting failure mechanisms affect each others performance, and thereby the system reliability. We describe such interactions in the context of flood defenses, and analyze under which conditions such interactions have a large impact on reliability using a Monte Carlo-based quantification method. We provide simple examples and an application to levee failure due to landward slope instability and backward erosion piping (BEP). The examples show that the largest interaction effects are expected when the trigger mechanism is relatively likely to occur and the affected mechanism has a relatively large contribution to the system reliability. For the studied levee example, interactions between slope instability and BEP increased the failure probability up to a factor 4. Implications for the assessment and design of flood defenses are discussed.

1. Introduction

Reliability analysis is a crucial part of the management of infrastructure, in particular when large risks are involved when structures fail. Flood protection infrastructure such as levees, dams and storm surge barriers need to have high levels of reliability to provide sufficient safety against catastrophic flooding. Reliability analysis methods are used to quantify their current performance and expected future performance under changing conditions [1,2]. As such, it is an important component of risk-based management of flood protection systems [3,4]. To quantify flood defense reliability, engineers analyze the likelihood of failure mechanisms such as overtopping erosion or slope instability separately. In a system reliability analysis, these failure mechanisms and different sections are combined considering dependence between random variables in all sections and mechanisms [5]. However, such failure processes can also affect each other [6], and thereby change the reliability compared to the case of independent failure processes. An example of such a physical interaction in the context of flood defenses is a shallow slope failure in a wide dam or levee during high water, which may not lead to complete instability of the structure, but decreases the erosion resistance of the landward slope against overtopping [7].

In line with definitions in the literature [8–10] interaction is defined here as follows: an interaction occurs if the occurrence of a (influencing) mechanism changes certain system parameters which trigger or prevent failure of other (affected) mechanisms. Although the individual mechanisms alone might not result in system failure due to additional resistance after one of them occurs, the causal dependencies between the two mechanisms can lead to failure [6]. The interaction can lead to immediate failure of the affected component, or to an immediate strength reduction which may lead to failure at a later moment. Interactions are defined as positive if they increase the other component's failure probability, and negative if they decrease it [9]. These interaction effects on reliability have been described using different terms such as sequential failures [11,12], failure propagation [13], failure collaboration [14] or trigger effect [15].

It is important to note that dependence between failures of different components of a system can take different forms. Well-known dependencies are statistical correlations between the safety margins of components or failure mechanisms, which can arise from correlation between shared variables. For instance, the same parameter can affect multiple mechanisms (e.g., water level) or parameters can be related by nature (e.g., soil grain size and permeability). Similarly, spatial

* Corresponding author at: Department of Hydraulic Engineering, Delft University of Technology, Delft, Netherlands.
E-mail address: j.c.pol@tudelft.nl (J.C. Pol).

https://doi.org/10.1016/j.ress.2022.108987
Received 18 March 2022; Received in revised form 17 November 2022; Accepted 18 November 2022
Available online 21 November 2022

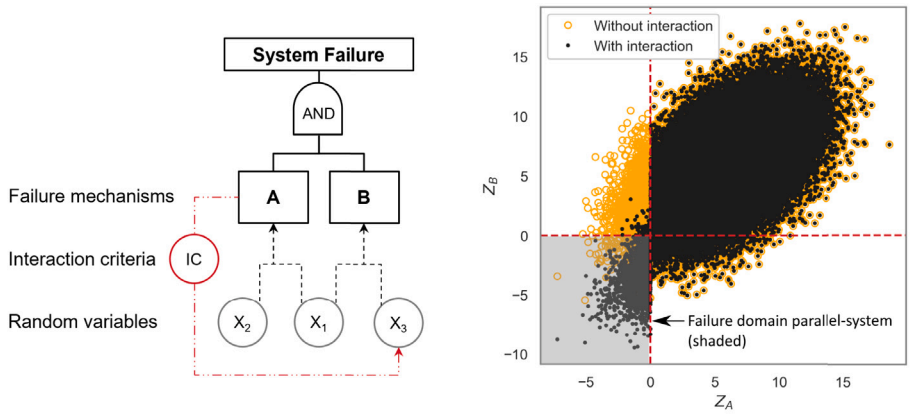

(a) 2-element parallel system where interaction IC reduces strength variable X_3.

(b) Safety margins Z_A and Z_B, with and without interaction.

Fig. 1. Example of an interaction in a correlated 2-element parallel system, such that the resistance of B decreases through X_3 if A fails.

correlations result in correlated elements. Such correlations have been analyzed for flood defense reliability [5,16]. The physical interactions between failure mechanisms studied in this paper are a different form of dependence, which arises from causal relationships between failure processes, but not from statistical correlation.

Fig. 1 shows an illustrative example of interaction, which is elaborated further in Section 3.2. Consider a parallel system of two failure mechanisms A and B depending on the variables $X_1 \ldots X_3$ (Fig. 1(a)). Due to the interaction IC, X_3 is affected by a given degree when A fails. The effect of the interaction appears as a change in Z_B if $Z_A < 0$ (Fig. 1(b)). This changes the probability that the system is in the failure domain, indicated by the shaded area. The difference between statistical correlation and physical interaction becomes clear from Fig. 1(b). In the scatterplot of the safety margins Z_A and Z_B, an interaction shows a discontinuity (at $Z_A = 0$ if A is the trigger), whereas statistical correlations do not. Statistical correlations are not the focus of this paper, but play a role as they affect the impact of interactions.

Such physical interactions are usually not considered in flood defense reliability, but have been analyzed in the context of reliability and degradation of mechanical systems [8–10,13–15,17,18] and load redistribution after local failures in complex structures [11,12,19,20]. In the studies on mechanical systems, the failure interaction is mostly caused by gradual or shock degradation of a component, and component performance data is available to calibrate degradation models. In contrast, failure of levees and dams is mostly driven by extreme events (shocks exceeding the strength capacity) instead of gradual degradation, and usually no data on degradation rates is available. Levee failure involves less interacting elements and less potential failure sequences compared to complex structures, which are often analyzed with branch-and-bound methods [11,19]. But an additional complexity for levees is that not only the sequence but also the timing of failure within a load event may be important for the failure behavior. Dams and offshore structures have similar failure characteristics as levees and were considered in some recent studies [21–23]. Pei et al. [23] analyzed the system reliability of a gravity dam with multiple sections and two failure mechanisms using Bayesian Networks, a failure path search and Monte Carlo Simulation. However, no physical interactions are considered between the two failure paths (strength and instability) for each dam section. Andreini et al. [21] analyzed the reliability of a dam subject to concentrated leak erosion with two events (erosion initiation and failed interventions) in one failure path, but no physical interaction between failure mechanisms. Adumene et al. [22] described interactions between environmental factors influencing corrosion rates of offshore structures using Bayesian Networks. They used Monte Carlo Simulation to quantify the failure probability, in which only statistical dependence between failure mechanisms is modeled but no physical interactions. Others quantified interactions based on expert judgment [24].

The main reason why interactions are neglected in levee reliability analysis, is because levees are often considered as series systems which fail if one of their failure mechanisms occur. In that case, failure paths consist of single failure mechanisms. Interactions are irrelevant in such a system definition because when the trigger mechanism occurs, the levee is assumed to fail anyway. However, there is an increasing interest in methods to make levee reliability assessments less conservative. One way is to distinguish different subsequent processes within a failure path [25]. Instead of assuming failure when a failure path initiates, one also quantifies the residual resistance after this initiating failure mechanism [26–30]. Accounting for these additional processes within a failure path can introduce physical interactions between these processes.

Interacting failures in flood defenses have not been studied before and are currently neglected in assessment and design. It is unclear to levee safety analysts under which conditions physical interactions between failure mechanisms can have a significant impact on the reliability of flood defenses and how these interactions can be included in reliability analyses. Therefore, this paper presents an application of reliability methods to flood defense infrastructure where different failure mechanisms interact. The main contributions are that the paper addresses the relevance of interacting failures for flood defense reliability, it shows what kind of interactions may occur in levees, how these can be included in reliability analyses and how these affect levee safety. The applied Monte Carlo framework is not new, but provides a flexible and robust method to quantify effects on reliability, even in cases where timing of failures has an influence. We analyze two conceptual examples and an example of a levee considering the failure mechanisms of landward slope instability and backward erosion piping. Although the paper focuses on flood defenses, the methods apply to a broader range of structures.

The remainder of the paper is organized as follows. Section 2 describes interactions between failure mechanisms in the context of flood defense reliability, including examples. Section 3 describes the reliability analysis method and the approach for application to the conceptual examples and a levee example. Section 4 presents the results of both examples, focusing on the conditions in which interactions are important. Section 5 discusses implications for application to flood defenses, and Section 6 presents the conclusions.

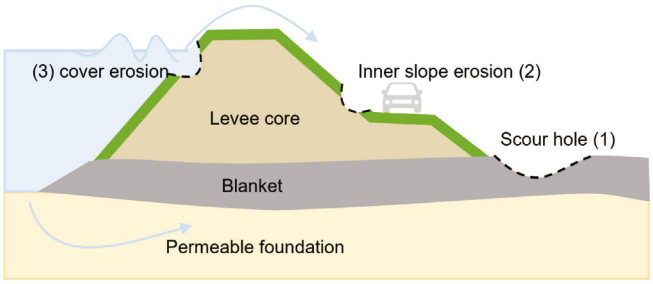

(a) Effects of external erosion.

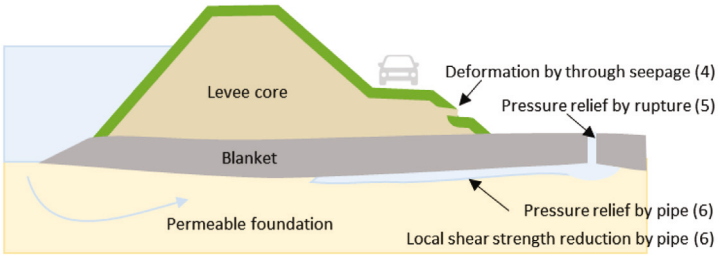

(b) Effects of internal erosion.

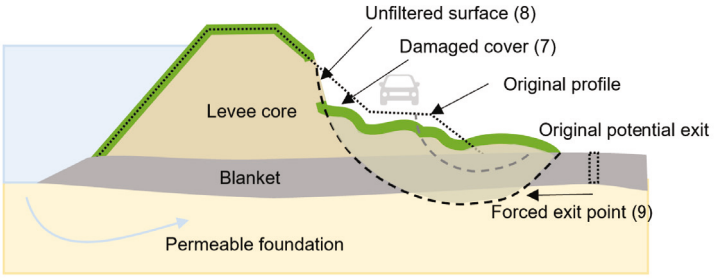

(c) Effects of slope instability.

Fig. 2. Illustration of interaction effects initiated by external erosion, internal erosion and slope instability. Numbers refer to interactions in Table 1.

2. Interactions in levee failure

2.1. Levee failure mechanisms and failure paths

As levees fail due to varying causes, engineers distinguish several failure mechanisms or failure modes. Examples are external erosion by overtopping, internal erosion by seepage, or slope instability. However, a levee can also fail by a combination of failure mechanisms occurring during the same event. Therefore, we first clarify some terminology related to failure mechanisms.

In this paper, we define *levee failure* as the state in which a levee fails to fulfill its primary function (flood prevention), i.e. when flooding occurs. Such a failure can follow from a breach or excessive overflow. We define a *failure path* as a chain of potential events leading to levee failure. These events may be physical processes related to failure of levee elements (e.g., grass cover erosion) or involve human actions (e.g., fail to detect damage and implement remedial action). The physical processes are commonly referred to as *failure mechanisms*, but it must be noted that in the context of this paper *failure mechanism* can refer to a part of the failure path, not necessarily to complete levee failure. Failure paths are also referred to as failure scenarios [6,31].

2.2. Physical interactions in levees

Although levee design considers distinct mechanisms, real levee failures can be a combination of different mechanisms. According to Özer et al. [32], in about 30% of the levee breaches during the 2002 and 2013 Elbe floods in Germany multiple failure mechanisms were observed. Another example is the London Avenue Canal South levee failure during Hurricane Katrina, where tilting of a flood wall seems to have increased underseepage and induced slope instability or backward erosion [33–35].

Table 1 lists possible interactions for levees grouped by the main failure mechanisms of external erosion (erosion by wave or flow impact on the levee cover), internal erosion (erosion by seepage flow through the levee) and slope instability. Fig. 2 illustrates the associated damages which may affect other mechanisms. Within the scope of this paper, we cannot give an exhaustive list of interactions in levees. Which interactions play a role will strongly depend on the levee characteristics. For instance, the presence of structural elements can introduce additional interactions due to unequal deformation of soil and structural elements. A more structured inventory of possible interactions can be obtained using influence diagrams relating the input parameters of failure mechanisms to their effects on levee elements.

2.3. Approaches to quantify interactions in levees

We see two main approaches to quantify failure mechanism interactions. Approach (**1**) couples the interacting processes in a process-based model. In a reliability analysis, this coupled model is then evaluated instead of the separate failure models. A few studies use such coupled

Table 1
Examples of interactions in earthen flood defenses (levees), grouped by external erosion, internal erosion and slope instability.

Number in Fig. 2	Trigger mechanism	Affected mechanism	Interaction description
1	External (wave overtopping)	internal (backward erosion)	Scour hole at the levee toe reduces the cover layer thickness, which increases chances of uplift, rupture, heave and backward erosion.
2	External (wave overtopping)	Internal (through-seepage)	Grass cover erosion induces seepage erosion from a sandy levee core with a high phreatic line, as the natural filter is removed (micro-instability).
3	External (wave attack)	Internal (through-seepage) & stability	Damage of outer slope low-permeability lining increases infiltration, which affects internal erosion and slope stability through higher phreatic levels.
4	Internal (through-seepage, animal burrows)	External (wave overtopping)	Seepage through the embankment due to high phreatic line (through-seepage or micro-instability), possibly in combination with animal burrows, leads to particle loss and deformation of the grass cover, which reduces its resistance against wave overtopping.
5	Internal (blanket rupture)	Stability	A vertical crack in the blanket layer and a horizontal pipe in the foundation reduces the aquifer head.
6	Internal (backward erosion)	Stability	Erosion lens or horizontal pipes in the foundation reduce aquifer pore pressures. It also reduces the shear strength at the interface of the aquifer and the blanket, although this occurs locally while slope failure occurs over a larger width (3D effects) [36].
7	Stability	External (wave overtopping)	Shallow slope failure damages the grass cover and creates a cliff, which reduces the resistance against wave overtopping [30].
8	Stability	Internal (through-seepage)	Shallow slope failure induces seepage through the embankment (micro-instability) by removing the cover which acts as a filter against sand transport.
9	Stability	Internal (backward erosion)	Deeper slope failure or deformation of a rigid structure induces a hydraulic shortcut through the blanket, which may change the seepage length [34].

models for internal erosion and slope stability [36–38]. Fu et al. [38] also applied the coupled model in a reliability analysis using MCS and a response surface. Approach (**2**) keeps the failure models separate, but incorporates the interactions in the reliability analysis by evaluating the failure models with adapted parameters, depending on the occurrence of a predefined trigger. This approach can be followed when the interactions can be defined as discrete events.

Approach (**2**) can be implemented in different ways, depending on the complexity of the interactions. The most simple way is scenario-based (**2a**), where different scenarios are defined for the occurrence of the trigger. Then the failure probability or the stochastic variables of the affected mechanisms are adapted for the scenarios in which the trigger occurs. Examples of this approach are event tree methods for the quantification of backward erosion piping risks [28] or slope instability [27]. Approach **2a** requires the analyst to predefine the sequence in which the events are ordered and analyzed. In case of interactions, one would place the trigger event first to be able to include the probability of other events given the trigger. However, the timing or sequence of events may be unknown and can have an important effect on the outcome. Consider the combination of grass cover erosion and slope instability. If the slope failure occurs before wave overtopping, it reduces the erosion-resistance of the grass cover. If overtopping occurs first, this strength reduction by slope failure is irrelevant. If the failure sequence is unknown, both options should be explored. If not only the sequence but also the timing of failures within the load event is important for the failure behavior, a more flexible approach (**2b**) is needed. The next section describes such a simulation-based approach, which is used for the examples in this paper.

3. Quantification method

3.1. Reliability method

Structural reliability analysis or probabilistic safety analysis aims to quantify the probability of failure P_F of a structure or system of structures [1,12,39]. The basic components for such a quantitative analysis are failure models, probability distributions of model parameters, and a reliability method to quantify the probability that the model parameters are in the failure domain. The general formulation of this problem is:

$$P_F = P(Z_{sys} \leq 0) = \int_{Z_{sys} \leq 0} f_{\mathbf{X}}(\mathbf{x}) d\mathbf{x} \tag{1}$$

Where the system safety margin $Z_{sys} = g(\mathbf{X})$, $Z_{sys} < 0$ defines failure, $g(.)$ denotes a failure model or limit state function (LSF), $\mathbf{X}$ is a vector of random variables, and $f_{\mathbf{X}}(\mathbf{x})$ is the joint probability density of the random variables. Classical methods to solve this problem are Monte Carlo Simulation (MCS) [40] and the First Order Reliability Method (FORM) [41].

The reliability method used to quantify the effect of interactions, is based on Monte Carlo Simulation (MCS) because of its flexibility and robustness. The flow chart in Fig. 3 presents the MCS framework, which is explained below. First, N_s random samples are generated for all stochastic variables $\mathbf{X}$, considering their marginal probability density functions (PDF) and the correlation between the variables. Variables which vary randomly in time during an extreme event (e.g., wind speed), need to be re-sampled for different time steps. Although the examples in this paper are limited to one element (e.g., levee cross section), the method is suitable for systems of multiple elements (N_e, see Fig. 3) with correlated variables. Stochastic variables $\mathbf{X}^{i,j,t}$ are drawn for each realization i, element j and time step t. Subsequently, the failure mechanism models $g(\mathbf{X})$ and the system (levee) safety margin Z^i_{sys} are evaluated. The interactions are included in the definition of the failure models, as is explained in more detail in the examples (Sections 3.2 and 3.3). Finally, the failure probability P_F is given by the fraction of samples in which system failure occurs ($Z^i_{sys} < 0$) over the total number of samples N_s. In this approach, interactions occur only within an element, not between elements [42]

3.2. Methods for conceptual examples

3.2.1. Failure models and failure definition

The conceptual analysis is performed for two simple systems: (1) a 2-element parallel system and (2) a series system of two 2-element parallel systems (Fig. 4). These examples are sufficiently simple to analyze analytically [43], yet can illustrate the effects of interactions.

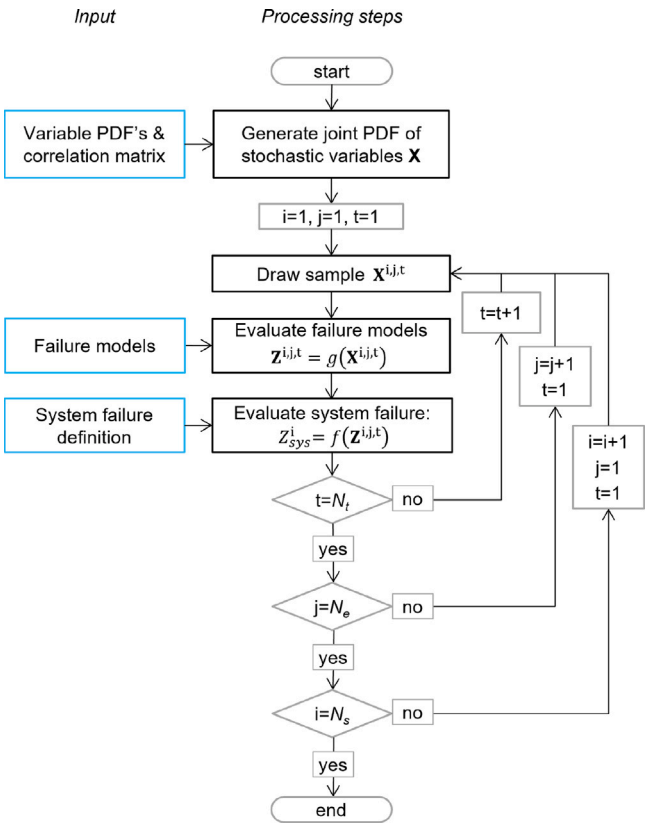

Fig. 3. Reliability method for interactions based on Monte Carlo Simulation.

Note that for the other simple case of a pure series system, interactions are not relevant as the system is assumed to fail if one of the potential triggers occurs.

In these examples, the failure mechanisms without interaction are described by simple limit state functions (LSF) of two normally distributed variables:

$$Z_A = X_2 - X_1 \tag{2}$$

$$Z_B = X_3 - X_1 \tag{3}$$

$$Z_C = X_4 - X_1 \tag{4}$$

$$Z_D = X_5 - X_1 \tag{5}$$

In this example, X_1 acts as load, $X_2 \ldots X_5$ as resistance, so the load is identical for each component. In the context of flood defenses, X_1 can be interpreted as water level and $X_2 \ldots X_5$ as the critical water level of each mechanism. All variables are time-invariant.

The interaction assumed in this example is a reduction (r_{int}) of the strength variable X_3 (for system 1) or X_5 (for system 2) which occurs if sub-mechanism A fails. The limit state functions including interactions are denoted by $\hat{Z}$ and are written as:

$$\hat{Z}_B = X_3(1 - r_{int} \cdot \mathrm{H}(X_1 - X_2)) - X_1 \tag{6}$$

$$\hat{Z}_D = X_5(1 - r_{int} \cdot \mathrm{H}(X_1 - X_2)) - X_1 \tag{7}$$

Here H(.) denotes the Heaviside unit step function, which returns 0 when the argument is negative and 1 when positive. Hence it can be used to make the LSF dependent on the exceedance of some threshold, for instance the failure threshold of a component.

System failure depends on the mechanism failures as defined by Eq. (8) (system 1) and Eq. (9) (system 2). In case of interactions, Z_B and Z_D are replaced by $\hat{Z}_B$ and $\hat{Z}_D$.

$$F_{sys1} = [Z_A < 0 \cap Z_B < 0] \tag{8}$$

$$F_{sys2} = [(Z_A < 0 \cap Z_B < 0) \cup (Z_C < 0 \cap Z_D < 0)] \tag{9}$$

3.2.2. Analyzed cases

The distributions of and correlation between variables are varied to obtain different degrees of correlation between the trigger and affected mechanism ($\rho_{(Z_A,Z_B)}$ for system 1) and different ratios of the failure probability of the trigger and affected mechanism (P_A/P_B). Section 4.1 analyzes these variations. All cases have $N_s = 10^5$ samples, $N_e = 1$ element, and $N_t = 1$ timestep.

System 1. The base case of system 1 is characterized by the following variables with mean μ and standard deviation σ: $X_1 \sim \mathcal{N}(\mu = 6, \sigma = 2)$ and $X_2 = X_3 \sim \mathcal{N}(12, 2)$, which are uncorrelated. Subsequently, cases are computed with different means and correlations compared to the base case. The correlation between the strength of the two mechanisms $\rho_{(X_2,X_3)}$ varies between 0, 0.5, 0.8 and 1. To obtain a factor 10 smaller and larger ratio P_A/P_B, μ_{X_3} respectively μ_{X_2} are set to 8.7 instead of 12. System 1 is analyzed with a strength reduction $r_{int} = 0.1$ (10%) and $r_{int} = 0.5$ (50%).

System 2. The base case of system 2 is characterized by the following variables: $X_1 \sim \mathcal{N}(6, 2)$ and $X_2 \ldots X_5 \sim \mathcal{N}(12, 2)$, which are uncorrelated. So, the base case has four failure mechanisms which have equal but uncorrelated strength distributions. Again, cases are computed with different means and correlations compared to the base case. The correlation within a subsystem ($\rho_{(X_2,X_3)} = \rho_{(X_4,X_5)}$) varies between 0, 0.5, 0.8 and 1. The correlation across subsystems ($\rho_{(X_2,X_4)} = \rho_{(X_3,X_5)}$) varies between 0, 0.5 and 1. Like for system 1, to obtain a factor 10 smaller and larger ratio P_A/P_D, the mean values $\mu_{X_3} = \mu_{X_5}$ respectively $\mu_{X_2} = \mu_{X_4}$ are set to 8.7 instead of 12. System 2 is analyzed with $r_{int} = 0.5$.

3.3. Methods for levee example

This section describes the methods used to analyze a simplified levee example, considering two failure paths: (1) a large slope instability and (2) blanket uplift and backward erosion piping. The considered interaction is number 9 in Table 1: initiation of blanket rupture by slope instability. Slope instability may occur at several positions in the levee, ranging from shallow slope failures near the landward toe to deep slope failures cutting through the waterside slope (Fig. 5). If the levee remains stable after an initial slope failure near the landward toe, no flooding occurs, but the blanket is still affected which may have an influence on the resistance against backward erosion piping (BEP). This influence takes two forms in this example. First, a sufficiently deep slip plane which cuts through the blanket creates a direct hydraulic shortcut through the blanket, so that uplift and rupture are not required anymore to initiate backward erosion. Second, the seepage length for BEP may change depending on the location where the slip plane intersects the blanket bottom. The modeling of the levee example follows the general framework in Fig. 3. The sections below explain specific modeling choices regarding (stochastic) variables, failure mechanism models and how interactions are included in these models.

3.3.1. Levee characteristics and Hydraulic loads

The impact of the interactions will strongly depend on the specific conditions, as will be shown in the conceptual examples (Section 4.1). To clearly illustrate the effect of interactions, the levee characteristics used in this levee example are realistic but are chosen in such a way that the impacts of interactions are relatively large. The levee has a sandy core which rests on a clay blanket layer with thickness D_{bl} on top of a homogeneous sandy aquifer with thickness D_{aq}. It has a

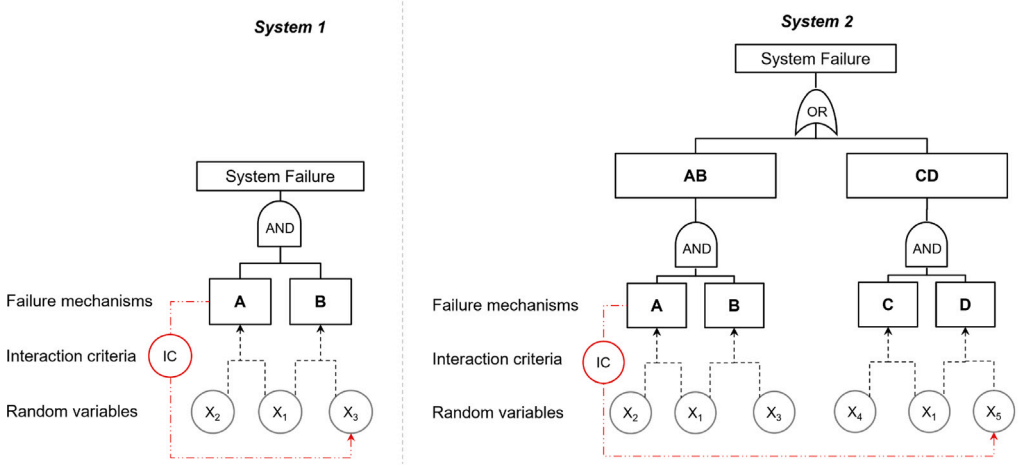

Fig. 4. Considered systems for conceptual examples. System 1: 2-element parallel system. System 2: Series system of 2 parallel systems.

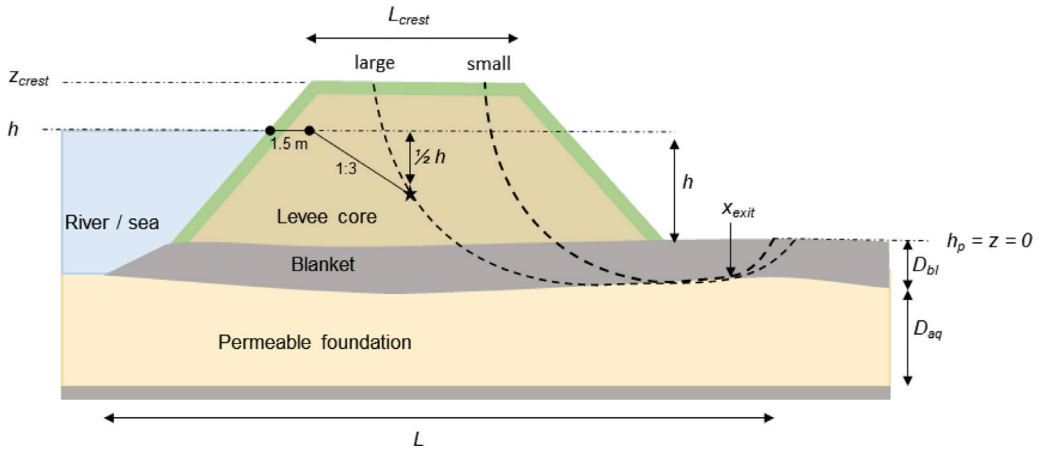

Fig. 5. Levee example: geometrical parameter definitions and slip plane scenarios (large, small).

landward slope of 1:2.5, riverside slope of 1:3, crest height z_{crest} = 5 m, and a crest width of L_{crest} = 12.5 m (Fig. 5). Table 2 shows the stochastic and deterministic variables used in the example. We assume that k_{aq} and d_{70} are correlated by a Gaussian copula with $\rho = 0.8$, and other variables are uncorrelated. The uncertainties in these variables are similar to values used in other studies on levee reliability in the Netherlands [27,44]. Some variables related to slope stability are modeled as deterministic to limit the number of random variables in this example. The model uncertainties are smaller than typically found in the literature for geotechnical models [45], in particular the slope stability uncertainty m_{sl} taken from [46]. Yet, it is noted that this value is used by default for levee assessment and design in the Netherlands and outcomes are generally in line with the experience of engineers and levee managers.

The failure analysis is conditioned on a range of peak water levels h_{max} between 3 and 5 m above reference level $z = 0$. The flood duration is also uncertain but in this example simplified to either a constant water level (case 1; see Section 3.3.5) or a deterministic trapezoidal hydrograph shape with base duration of 30 days at $h = 0$ and peak duration of 1 day at $h = h_{max}$ [47]. The 30 day flood event is discretized in timesteps of 12 h around the peak, and the failure processes are evaluated and updated in each time step. All variables are assumed to be constant within a time step. Strength variables are fully dependent between timesteps, and changes in water level are fully determined by the trapezoidal hydrograph shape.

3.3.2. Failure models: slope instability

Slope failure is assumed to occur if the stability factor F_S is smaller than 1. F_S is defined as the ratio of resisting forces and driving forces along the failure plane and is computed with a stability model as function of levee geometry, soil parameters and pore pressures. Then the limit state function for slope stability is defined as:

$$Z(t) = m_{sl} \cdot F_S(t) - 1 \tag{10}$$

where m_{sl} denotes the model uncertainty of the slope stability model, as given in Table 2.

Scenarios. Slope failure can occur along a large number of potential slip planes, which are a-priori unknown and depend on the specific combination of parameters. Therefore we use scenarios for the slip plane location. In this example there are only two scenarios: a large slip plane (SIL; Slope Instability Large) which leads to flooding, and a small slip plane (SIS) which does not lead to flooding because of a stable remaining profile but does cut through the blanket layer. A slip plane is assumed to lead to flooding if the location indicated by the star in Fig. 5 is part of it. This point is based on a minimal remaining width at the water line of 1.5 m to account for model uncertainty in the slip plane position, and a stable slope of 1:3 between the water level and the assumed height of the residual profile ($1/2h$). Note that failure along the small slip plane may also affect the stability of the large slip plane when water levels increase further during a high-water event. For instance because of a redistribution of weight, a reduction in soil strength at the slip surface or changes in pore water pressure. These effects on secondary slope failures are neglected in this example.

Table 2
Stochastic variables for levee example.

Variable	Symbol	Unit	Distr.	μ	σ
Hydraulic loads:					
Base duration		Days	Det.	30	
Peak duration		Days	Det.	1	
Seepage and Uplift:					
Seepage length	L	m	Logn.	60	5
Aquifer thickness	D_{aq}	m	Logn.	25	5
Blanket thickness	D_{bl}	m	Logn.	5	0.25
Conductivity aquifer	k_{aq}	m/s	Logn.	$1 \cdot 10^{-4}$	$0.5 \cdot 10^{-4}$
Conductivity blanket	k_{bl}	m/s	Logn.	$1 \cdot 10^{-6}$	$0.5 \cdot 10^{-6}$
Model error uplift	m_u	–	Logn.	1	0.05
Backward Erosion Piping:					
Grain size	d_{70}	mm	Logn.	0.180	0.036
Angle of repose	θ	∘	Det.	37	
Constant White	η	–	Det.	0.25	
Particle density	ρ_s	kg/m^3	Det.	2650	
Model error BEP	m_p	–	Logn.	1	0.12
Slope instability:					
Sand, friction angle	ϕ'_s	∘	Det.	27	
Sand, cohesion	c'_s	kPa	Det.	0	
Sand, sat. weight	$\gamma_{sat,s}$	kN/m^3	Det.	20	
Sand, unsat. weight	$\gamma_{u,s}$	kN/m^3	Det.	18	
Clay, shear strength ratio	S	–	Logn.	0.25	0.03
Clay, strength exponent	m_{cl}	–	Det.	0.8	
Clay, pre-overburden pressure	POP	kPa	Det.	21.85	
Clay, sat. weight	$\gamma_{sat,cl}$	kN/m^3	Logn.	18	1
Model error Uplift-Van	m_{sl}	–	Logn.	1.005	0.033

Stability model. We use the D-Stability (version 2021.02) Limit Equilibrium Model [48] to determine the stability factor for a given input parameter combination. As uplift plays an important role in the interaction, we use the Uplift-Van slip plane model, of which the slip plane has a horizontal part bounded by two circular parts [49]. Soil strength in sandy layers is modeled with Mohr–Coulomb and in clay layers with SHANSEP [50]. For the large slip plane scenario, we force the slip plane position sufficiently close to the water side using a forbidden line between the star in Fig. 5 and the landward slope. The small slip plane is forced to cut the blanket using the tangent lines option in D-Stability.

Surrogate model. The large number of D-Stability model evaluations in a MCS analysis requires long computation times. A surrogate model replaces a complex process model (here: D-Stability) by a simpler model which can be quickly evaluated [51,52]. This allows to maintain the robust MCS approach while reducing the computation time. In this example we use multivariate linear interpolation as a very simple surrogate model to obtain stability factors for each realization. More advanced methods were also tested (Lasso Regression and Gaussian Process Regression) but linear interpolation is sufficient for this example. Predictor variables used in the stability surrogate model are: water level h, soil strength of blanket S, leakage length λ, blanket weight $\gamma_{sat,bl}$ and blanket thickness D_{bl}. λ includes the combined effect of k_{aq}, k_{bl}, D_{aq} and D_{bl} on the aquifer head: $\lambda = \sqrt{k_{aq} D_{aq} D_{bl} / k_{bl}}$. In cases with a time varying water level $h(t)$ in combination with a delay dt in slope failure with respect to the water level (see Section 3.3.5), the stability factor at time t is computed with the water level at time $t - dt$. Then, the stability factor for each slip plane given a sample of the stochastic variables is:

$$F_{s,\mathrm{i}}(t) = \mathcal{M}_{\mathrm{i}}(h(t-dt), S, \gamma_{sat,bl}, D_{bl}, \lambda) \tag{11}$$

where i denotes the slip plane scenario (SIS for small and SIL for large) and $\mathcal{M}$ denotes the surrogate model for the stability factor. Apart from the stability factor, the position where the slip plane cuts the blanket bottom (x_{exit}, see Fig. 5) is of interest for the interaction with piping, as it changes the seepage length (Eq. (17)). x_{exit} depends on the slip plane position and blanket–aquifer interface, and is only computed for the small slip plane. Similar to Eq. (11), the change in exit location Δx_{exit} is expressed as function of blanket thickness and the water level corresponding to the occurrence of the small slope failure $h(t_{SIS} - dt)$ where t_{SIS} is the time at which the small slope failure occurs:

$$\Delta x_{exit} = \mathcal{M}_{exit}(h(t_{SIS} - dt), D_{bl}) \tag{12}$$

The training dataset is composed of all combinations spanning the entire parameter space, with the following ranges of each predictor: $h = \{2, 3, 4, 5\}$ m, $S = \{0.18, 0.20, \ldots, 0.30\}$, $\lambda = \{50, 100, \ldots, 250\}$ m, $\gamma_{sat,bl} = \{13, 14, \ldots, 19\}$ kN/m^3, $D_{bl} = \{4.0, 4.5, 5, 5.5\}$ m. This gives 3920 combinations to evaluate in D-Stability.

3.3.3. Failure models: uplift and BEP

The response of the aquifer head to an increased water level is modeled according to Eq. (13), which is equivalent to case 7a from the USACE blanket theory [53] or model 4 A from Dutch guidelines [54]. This solution is based on horizontal flow in a leaky aquifer, vertical flow (leakage) through the blanket, an infinitely long polder blanket and no riverside blanket:

$$\varphi(x) = \varphi_{polder} + (h - \varphi_{polder}) \frac{\lambda}{L + \lambda} e^{-x/\lambda} \tag{13}$$

where φ denotes the aquifer head, x the distance from the landward toe, L the seepage length, and $\lambda = \sqrt{k_{aq} D_{aq} D_{bl} / k_{bl}}$ the polder side leakage length. In our example, $\varphi_{polder} = 0$ m.

Rupture of the blanket is assumed to occur if the aquifer head is larger than the blanket weight (uplift). This model is simply a vertical equilibrium and neglects additional resistance of the soil against tension or shear:

$$Z_{UPL}(t) = m_u \cdot I_u(t) \cdot D_{bl} \cdot (\gamma_{sat,bl} - \gamma_{water}) / \gamma_{water} - (\varphi_{lt}(t) - h_p) \tag{14}$$

In which m_u denotes the uplift model uncertainty factor [–], D_{bl} the blanket thickness [m], $\gamma_{sat,bl}$ and γ_{water} the weight of the blanket and water [kN/m^3], and h_p the polder water level [m]. $I_u(t) = \mathrm{H}(\min_{0\ldots t}\left[Z_{SIS}(t)\right])$ is an indicator based on the Heaviside unit step function and equals 1 if the blanket is intact and 0 if ruptured by the interaction with the small slope failure which cuts through the blanket layer. It considers the minimum of Z_{SIS} over the interval $0\ldots t$ because the effects of a slope failure will remain in later time steps.

The backward erosion piping (BEP) limit state is the difference between critical head difference H_c and applied head difference $h - h_p$:

$$Z_{BEP}(t) = H_c(t) - (h(t) - h_p) \tag{15}$$

where H_c is modeled with the revised Sellmeijer model [55]:

$$H_c(t) = m_s \cdot \hat{L}(t) \cdot \eta \frac{\rho_s - \rho_w}{\rho_w} \tan\theta \frac{d_{70}}{\sqrt[3]{\kappa \hat{L}(t)}} \left(\frac{d_{70,m}}{d_{70}}\right)^{0.6} 0.91 \times \left(\frac{D_{aq}}{\hat{L}(t)}\right)^{\frac{0.28}{\left(\frac{D_{aq}}{\hat{L}(t)}\right)^{2.8} - 1} + 0.04} \tag{16}$$

In which ρ_s and ρ_w denote the sediment and water density [kg/m^3], η the coefficient of White [–], θ the angle of repose [deg], d_{70} the grain size [m], κ intrinsic permeability [m^2], D_{aq} aquifer thickness [m]. $d_{70,m} = 2.08 \cdot 10^{-4}$ m and m_s is the model uncertainty factor of the Sellmeijer model. $\hat{L}$ is the seepage length including a possible shift Δx_{exit} in exit location due to the interaction with a small slope instability which cuts through the blanket:

$$\hat{L}(t) = L + \Delta x_{exit} \cdot \mathrm{H}(\min_{0\ldots t}(-Z_{SIS}(t))) \tag{17}$$

Δx_{exit} is given by Eq. (12) and Z_{SIS} by Eqs. (10) and (11).

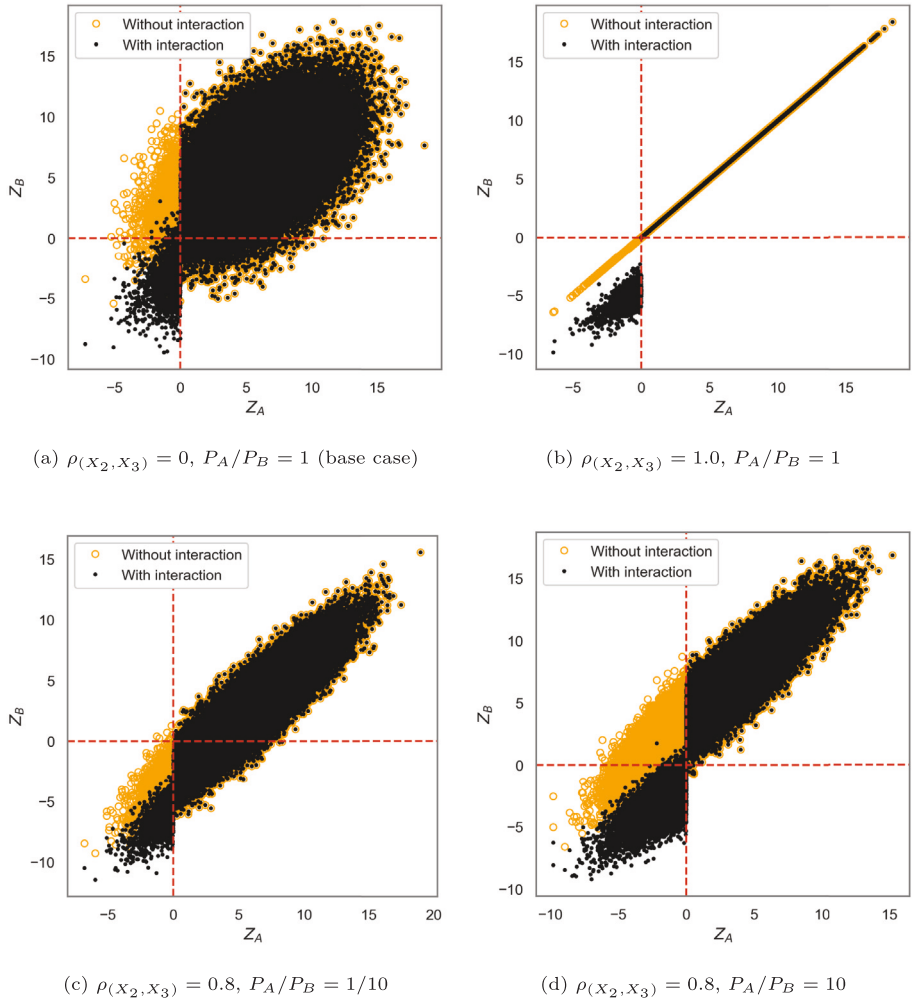

(a) $\rho_{(X_2,X_3)} = 0$, $P_A/P_B = 1$ (base case)

(b) $\rho_{(X_2,X_3)} = 1.0$, $P_A/P_B = 1$

(c) $\rho_{(X_2,X_3)} = 0.8$, $P_A/P_B = 1/10$

(d) $\rho_{(X_2,X_3)} = 0.8$, $P_A/P_B = 10$

Fig. 6. Z-Z plots for system 1 with 50% reduction of X_3; plots show examples for different correlations $\rho_{(X_2,X_3)}$ and ratios of component probabilities P_A/P_B. Interactions occur where black points deviate from the original yellow points. The failure domains are the bottom-left quadrants, where both $Z_A < 0$ & $Z_B < 0$.

3.3.4. System failure definition

In this example, there are two failure paths: either a large slope failure (SIL) or the joint occurrence of uplift (UPL) and backward erosion piping (BEP). Therefore, system failure F_{levee} is defined as the event when:

$$F_{levee} = \left[Z_{SIL} < 0 \cup \left(Z_{UPL} < 0 \cap Z_{BEP} < 0\right)\right] \tag{18}$$

When considering a time-varying water level this becomes:

$$F_{levee} = \left[\min_{0\ldots t}(Z_{SIL}) < 0 \cup \left(\min_{0\ldots t}(Z_{UPL}) < 0 \cap \min_{0\ldots t}(Z_{BEP}) < 0\right)\right] \tag{19}$$

3.3.5. Analyzed cases

Four sub-cases of this levee example are considered, which differ with respect to the timing of slope failures. Levee case 1 is the base case and has a constant water level. Levee case 2 has a time-varying water level as described in Section 3.3.1. Levee cases 3 and 4 have a time-varying water level and uncertainty in the timing of the small slope failure, represented by a failure delay dt_{SIS}. In levee case 3, $dt_{SIS} \sim \mathcal{N}(0, 48)$ h. So on average, the SIS failure occurs at the same water level as in case 1. In levee case 4, $dt_{SIS} \sim \mathcal{N}(96, 48)$ h, so the SIS failure is on average 96 h later than in the instantaneous case 1.

4. Results

4.1. Results of conceptual examples

The conceptual examples aim to investigate under which conditions interactions may have a significant influence on the system failure probability. For instance, the degree of correlation between the components, and the ratio between the component probabilities may influence the effect of the interaction. These examples follow the quantification method of Section 3.1, with the simplification of only one system-element and one time step.

We express the effect of interactions as the factor $f_{int} = P_{F,int}/P_{F,org}$, where $P_{F,int}$ and $P_{F,org}$ are the system failure probabilities with and without considering interactions, respectively. Furthermore, P_A is used as shorthand for the probability $P(Z_A < 0)$, and likewise P_B, P_C and P_D.

4.1.1. Results system 1 (2-element parallel)

The 2-element parallel system illustrates some basic probabilistic aspects regarding the contribution of interactions in the total failure probability. Of course, the magnitude of the interaction effect is an important determinant for the effect of interactions on the failure probability. In this example we use a 10% and 50% reduction on strength variable X_3. This analysis focuses on the probabilistic aspects, which determine how frequent this strength reduction occurs and to which extent that affects the total failure probability. As described

Table 3
Results of conceptual analysis system 1 (2-element parallel). Interaction effect f_{int} for different values of P_A/P_B and $\rho_{(X_2,X_3)}$. Base case result in boldface.

P_A/P_B	50% reduction of X_3				10% reduction of X_3			
	$\rho_{(X_2,X_3)}$				$\rho_{(X_2,X_3)}$			
	0	0.5	0.8	1	0	0.5	0.8	1
1/10	1.6	1.1	1	1	1.2	1.1	1	1
1	**6.3**	2.8	1.7	1	1.7	1.6	1.4	1
10	14	11	10	10	2.1	2.0	2.1	2.1

in Section 3.2, the variable means and correlations were varied to illustrate how these variations influence the interaction effect f_{int}.

The results of the base case of system 1 are illustrated in Fig. 6(a), which shows the component Z-values with (black) and without (orange) interaction. The weakening due to the interaction appears as a shift in the point cloud. Without interaction, the component probabilities are $P_A = P_B = 0.017$ and the system failure probability $P_{F,org} = P(A \cap B) = 0.0026$ (portion of realizations in the bottom-left quadrant). The interaction triggered by $Z_A < 0$ (with a 50% strength reduction of X_3) decreases the safety margin Z_B, so that P_B increases to 0.031 and $P_{F,int} = 0.016$. Consequently, the interaction effect $f_{int} = 6.3$ for the base case. Now, the ratio between component reliability P_A/P_B and the correlation between the two strength variables $\rho_{(X_2,X_3)}$ are varied. Table 3 presents the resulting interaction effects f_{int}. Some of these cases are illustrated in Fig. 6.

First we discuss the influence of correlation between the strength of the two elements $\rho_{(X_2,X_3)}$. Table 3 shows that the stronger this correlation, the smaller the effect of an interaction. This is illustrated in comparing Figs. 6(a) and 6(b). The smaller the correlation $\rho_{(X_2,X_3)}$, the less samples fail both on mechanism A and B, and therefore more samples can be moved to the failure domain by the interaction. In the fully correlated case with equal component probabilities ($P_A = P_B$, Fig. 6(b)), P_F is not affected by the interaction. This is because all samples with $Z_A < 0$, which triggers the interaction, are already in the failure domain. The same holds when $P_A < P_B$ in the fully correlated case. However, if $P_A > P_B$, there is an effect of interaction in the fully correlated case. This is caused by the samples with $Z_A < 0$ and $Z_B > 0$ without interaction, which fail due to the weakening by the interaction ($Z_B < 0$ with interaction).

Second, we discuss the influence of the ratio P_A/P_B. Table 3, Figs. 6(c) and 6(d) show that the smaller the failure probability of B (the affected) compared to A (the trigger), the larger the interaction effect. If B is already relatively weak without interaction ($P_B \gg P_A$), the conditional probability $P(B|A)$ is close to 1, and further weakening by the interaction will not affect the system probability (Fig. 6(c)). Furthermore, the influence of correlation depends on P_A/P_B. In case of $P_A/P_B = 1$ this influence is relatively large, whereas for $P_A/P_B = 1/10$ and $P_A/P_B = 10$ one needs a very low correlation (<0.5) to observe a significant change in f_{int} (Table 3).

4.1.2. Results system 2 (series system of two parallel sub-systems)

Compared to system 1, system 2 is more realistic for levee cross sections. The two subsystems of system 2 can be seen as failure paths which each consist of two failure mechanisms. For instance that a levee fails if either rupture and backward erosion both occur, or slope failure and overtopping erosion both occur. Unlike in system 1, system failure is not only the result of the trigger mechanism and affected mechanism (A and D), but additional mechanisms (B and C) play a role too. Also for system 2 the impact of the interaction on the system reliability is calculated with different values of the variable means and correlations.

The results of the base case of system 2 are illustrated in Fig. 7. Without interaction, all component probabilities are 0.017 and the system failure probability $P_{F,org} = 0.0051$. The interaction triggered by $Z_A < 0$ decreases the safety margin Z_D (shift in Fig. 7(a)), so that P_D increases to 0.03 and $P_{F,int} = 0.0064$. Consequently, the interaction

Table 4
Results conceptual analysis system 2. Table shows interaction effect f_{int} for different ratios of component probabilities P_A/P_D and different values of $\rho_{(X_2,X_3)} = \rho_{(X_4,X_5)}$ (correlation within subsystems) and $\rho_{(X_2,X_4)} = \rho_{(X_3,X_5)}$ (correlation between subsystems). Base case result in boldface.

	50% reduction of X_5			
	$\rho_{(X_2,X_3)}$ and $\rho_{(X_4,X_5)}$			
	0	0.5	0.8	1.0
P_A/P_D	AB and CD uncorrelated: $\rho_{(X_2,X_4)} = 0$			
1/10	1.0	1.0	1.0	1.0
1	**1.25**	1.05	1.02	1.0
10	3.7	2.8	2.6	2.6
P_A/P_D	AB and CD correlated: $\rho_{(X_2,X_4)} = 0.5$			
1/10	1.06	1.0	1.0	1.0
1	1.8	1.2	1.0	1.0
10	5.6	4.0	3.7	3.6
P_A/P_D	AB and CD correlated: $\rho_{(X_2,X_4)} = 1$			
1/10	3.4	1.1	1.0	1.0
1	3.2	2.8	1.7	1.0
10	15	11	9.3	9.4

effect $f_{int} = 1.25$ for the base case of system 2. This interaction effect is considerably smaller than in the base case of system 1 ($f_{int} = 6.3$). The shifted points also appear in Fig. 7(b), but here show no discontinuity as the change is independent of the occurrence of C. This is due to the system architecture where the interaction affects only one of the parallel mechanisms (D) of the subsystem CD (Fig. 4). For low correlations between AB and CD (i.e., small $\rho_{(X_2,X_4)}$), the probability is small that A and C fail together, so in most cases that the interaction from A to D occurs, $Z_C > 0$ so C will be strong enough to prevent the failure path CD (Fig. 7(b)).

The results of the variations in P_A/P_D and the correlations between strength variables are shown in Table 4, and some are illustrated in Fig. 8. Comparing Tables 3 and 4 shows that also in system 2, the effects of interaction f_{int} are higher for lower correlation within a subsystem ($\rho_{(X_2,X_3)}$), and for larger ratios between the probability of the trigger and affected mechanism (P_A/P_D). The effect of correlation within a subsystem ($\rho_{(X_2,X_3)}$) is illustrated in comparing Figs. 7(b) and 8(a). Regarding the influence of P_A/P_D, compare Figs. 8(c) and 8(d). In case of $P_A/P_D = 10$ the trigger occurs more often than when $P_A/P_D = 1/10$, resulting in larger effects of interaction on the system reliability.

The effect of correlation between the two subsystems AB and CD is indicated by varying $\rho_{(X_2,X_4)}$. If AB and CD are strongly correlated (i.e. large $\rho_{(X_2,X_4)}$), failure of C is more likely in case of failure A. This results in more interactions occurring in the failure domain of C and D (compare Figs. 7(b) and 8(b)). Therefore, f_{int} is larger when AB and CD are correlated. In practice, AB and CD will often represent different failure paths with different processes and variables involved, so correlation between those subsystems is expected to be limited.

4.2. Levee example results

To demonstrate the effects of interactions for a realistic case, we analyzed the reliability of a levee with properties as shown in Table 2. Levee failure depends on four failure mechanisms: slope instability small (SIS) which cuts through the blanket but does not lead to levee failure, slope instability large (SIL) which directly leads to levee failure, blanket uplift (UPL) and backward erosion piping (BEP) which in combination lead to levee failure. The effect of interaction on the failure probability is illustrated for case 1 (constant water level) and a relatively high water level $h_{max} = 4$ m (Table 5 and Fig. 9).

Table 5 show that without interaction, the levee failure probability P_F is dominated by the large slope failure ($P_F \approx P_{SIL}$). The failure path of joint occurrence of uplift and BEP has a much lower probability

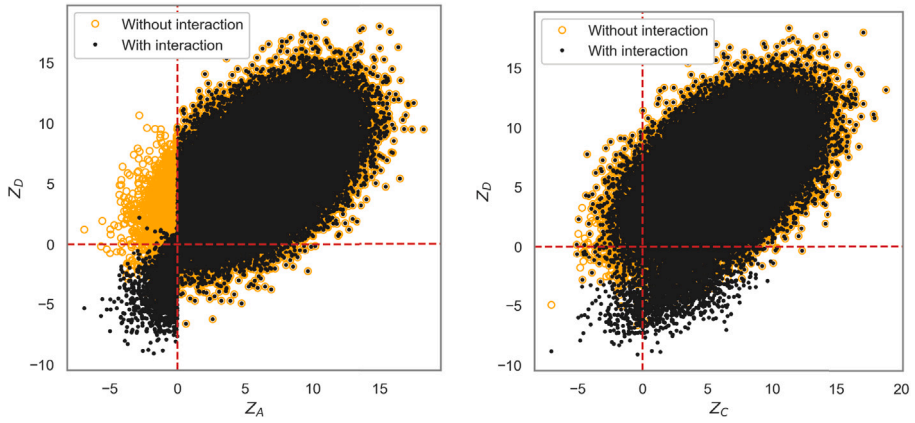

(a) Z_A and Z_D (b) Z_C and Z_D

Fig. 7. Z-Z plots for system 2 base case with $\rho_{(X_2,X_3)} = 0$, $\rho_{(X_2,X_4)} = 0$ and $P_A = P_B = P_C = P_D$. Influencing mechanism is A, affected mechanism is D. Interactions occur where black points deviate from the original yellow circles. The failure domain where $Z_C < 0$ & $Z_D < 0$ is the bottom-left quadrant of Fig. 7(b).

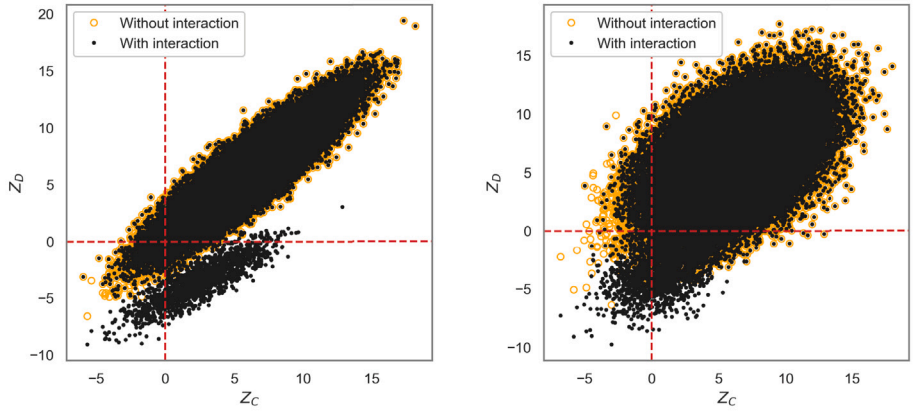

(a) $\rho_{X_2,X_3} = 0.8$, $\rho_{(X_2,X_4)} = 0$, $P_A/P_B = 1$ (b) $\rho_{X_2,X_3} = 0$, $\rho_{(X_2,X_4)} = 0.5$, $P_A/P_B = 1$

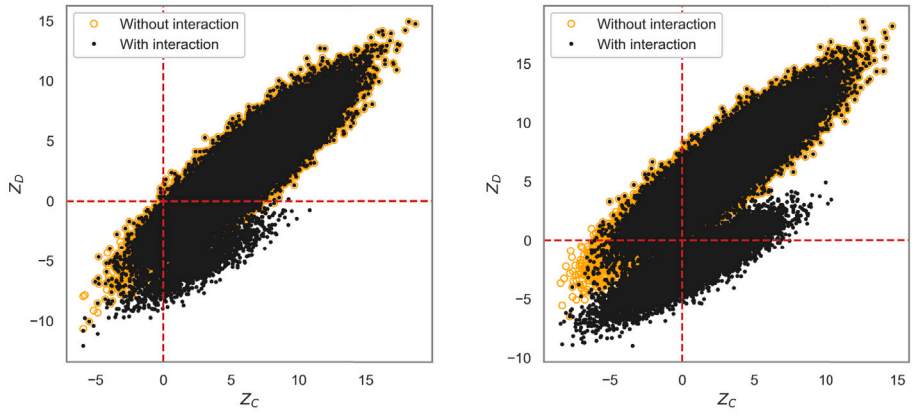

(c) $\rho_{X_2,X_3} = 0.8$, $\rho_{(X_2,X_4)} = 0$, $P_A/P_B = 0.1$ (d) $\rho_{X_2,X_3} = 0.8$, $\rho_{(X_2,X_4)} = 0$, $P_A/P_B = 10$

Fig. 8. $Z_C - Z_D$ plots for system 2 with 50% strength reduction of X_5, for different combinations of $\rho_{(X_2,X_3)}$ (correlation within subsystems), $\rho_{(X_2,X_4)}$ (correlation between subsystems) and $P_A/P_B = P_C/P_D$. Interactions occur where black points deviate from the original yellow circles. The failure domain where $Z_C < 0$ & $Z_D < 0$ is the bottom-left quadrant.

and contributes only marginally to P_F. After including the interaction triggered by SIS, the uplift probability increases strongly ($P_{UPL} \approx P_{SIS}$). The BEP probability decreases due to the changing L, but this effect is minor. The increased uplift probability increases the system failure probability P_F by a factor 2.6.

Fig. 9 visualizes the realizations Z of combinations of failure mechanisms, and how these change due to the interaction. The small and large slope failures (Fig. 9(a)) are not affected by the interaction, so the Z-values and mechanism probabilities do not change. The interaction triggered by SIS is clearly visible in the decreased uplift resistance Z_{UPL}

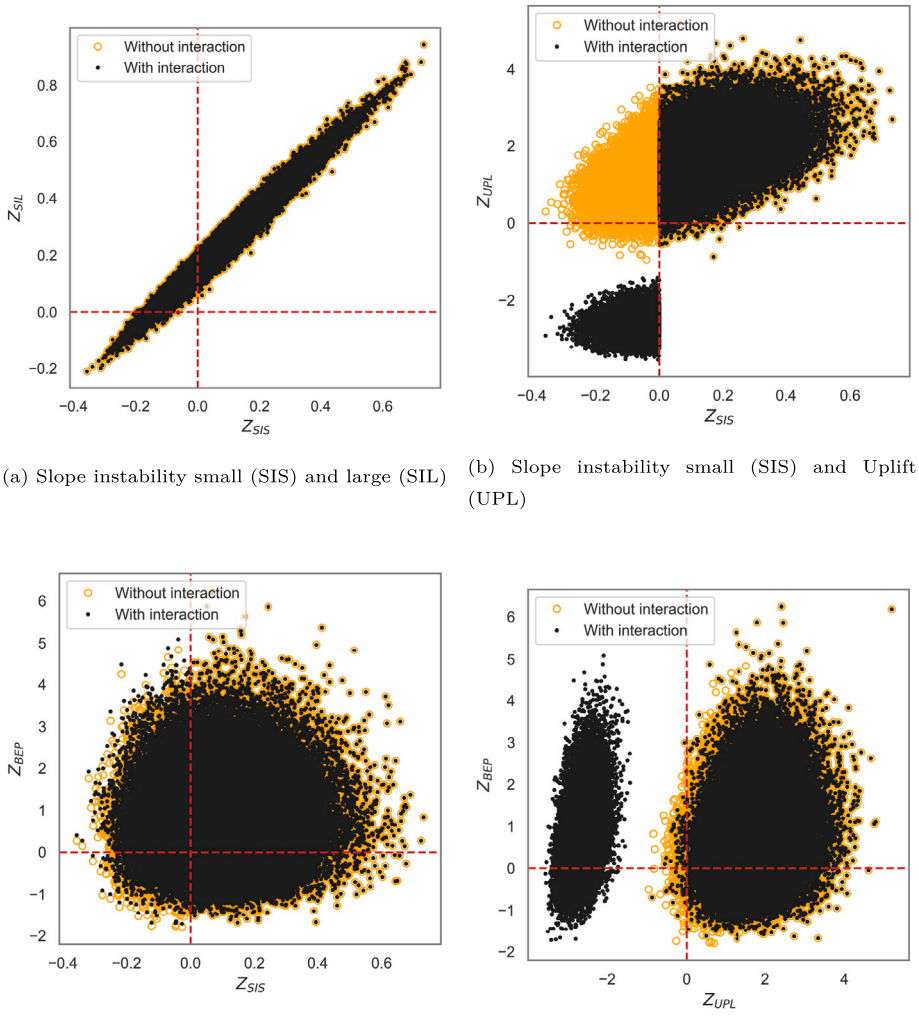

(a) Slope instability small (SIS) and large (SIL)

(b) Slope instability small (SIS) and Uplift (UPL)

(c) Slope instability small (SIS) and Backward erosion (BEP)

(d) Uplift (UPL) and Backward erosion (BEP)

Fig. 9. Z-Z plots of different levee failure mechanisms for case 1 (constant water level) and h = 4 m. Interactions occur where black points deviate from the original yellow circles. The failure domain consists of two parts: where both $Z_{SIS} < 0$ & $Z_{SIL} < 0$, and where both $Z_{UPL} < 0$ & $Z_{BEP} < 0$.

Table 5
Failure probabilities for levee example case 1 (constant water level), conditional on water level h_{max} = 4 m.

	P_{SIS}	P_{SIL}	P_{UPL}	P_{BEP}	$P_{Failure}$
Without interaction	0.24	0.020	0.0039	0.18	0.021
With interaction	0.24	0.020	0.24	0.17	0.054
Ratio	1	1	62	0.94	2.6

for all realizations where $Z_{\text{SIS}} < 0$ (Fig. 9(b)), which increases the uplift probability from 0.0039 to 0.24. Similarly, the interaction changes the BEP resistance Z_{BEP} by changing the seepage length L but the effect is hardly visible (Fig. 9(c)). The decrease in uplift resistance in part of the samples also appears in Fig. 9(d). Because this decrease is not related to Z_{BEP}, it appears as a shifted point cloud. Levee failure occurs if both UPL and BEP fail, so the bottom left quadrant of Fig. 9(d). Fig. 9(d) shows that the number of samples in this failure domain strongly increases due to the interaction.

Fig. 10 shows the resulting failure probabilities of case 1 conditional on a range of water levels (fragility curves). The magnitude of the interaction effect f_{int} varies with water level (Fig. 11) because the ratios of mechanism probabilities vary. In this example, the effect of interaction is significant (up to a factor 4 increase in failure probability), which is in line with the findings from the conceptual examples: the trigger (SIS) has a relatively high probability and the affected mechanism (UPL) is the strongest link in the failure path of uplift & BEP. Note that a similar levee case with a much lower SIS or BEP probability may show no significant interaction effect.

The effect of timing is shown by the cases 1–4 in Fig. 11. A time-varying water level (case 2) gives a slightly higher interaction effect (f_{int}) than a constant water level (case 1). Although the failure processes respond instantly to the water level, the small slope failure in case 2 can occur at lower levels than h_{max}. And the lower the water level at SIS failure, the closer to the levee will be the slip plane position. Hence the effect of interaction is larger. Adding uncertainty to the timing of the small slope instability (case 3) hardly affect the results. An additional delay in the timing of SIS by 96 h (case 4) results in lower interaction effects, up to a factor 3.4 instead of 4.2. This lower f_{int} is expected, as more SIS failures occur after the flood peak. In these post-peak failures, the maximum water level applied to BEP is lower than h_{max}, and hence P_{BEP} increases less due to the blanket rupture triggered by SIS. These results show that timing aspects can influence the interactions effect.

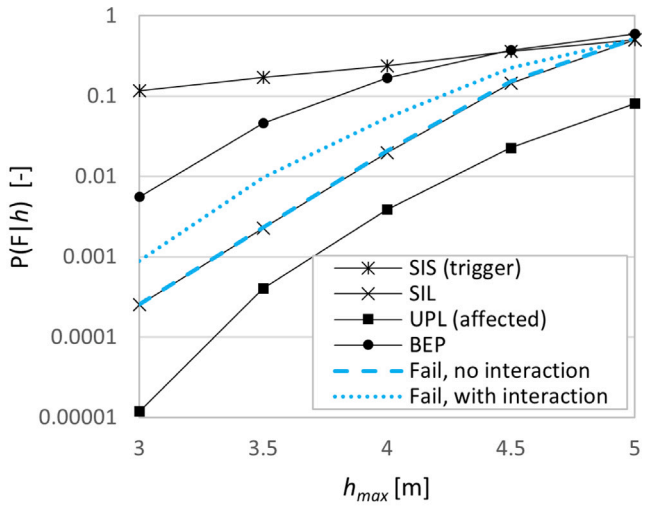

Fig. 10. Failure probabilities conditional on water level (fragility curve) per mechanism for levee case 1, including the combined levee failure probability ('Fail') with and without interaction. Slope instability small (SIS) and large (SIL), uplift (UPL) and backward erosion piping (BEP). Interaction effect f_{int} is the ratio between the dotted and dashed blue lines, see Fig. 11.

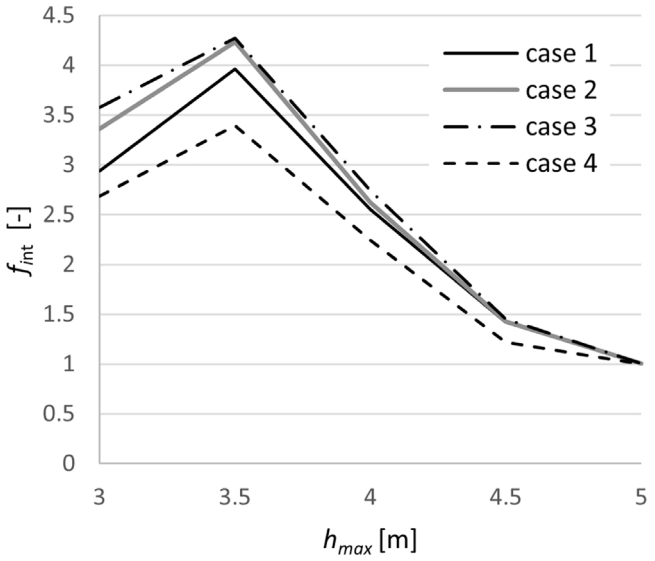

Fig. 11. Interaction effect f_{int} as function of peak water level h_{max} for case 1 (constant water level), and for time-varying water level with different degrees of delay in SIS failure (cases 2-4).

5. Discussion

5.1. When are interactions relevant?

For practical applications it may be useful to estimate in an early stage whether interactions are important for the system failure probability, before doing extensive simulations. The conceptual analysis shows that many factors affect the degree to which interactions matter. Three main factors are: (1) the criticality or importance of the affected component (mechanism) to the system reliability, (2) the degree to which this mechanism is affected by interactions, and (3) the probability that the trigger occurs.

These main factors depend on other factors. For instance, the importance of the affected mechanism depends on the system configuration, ratio of mechanism probabilities and correlation between mechanisms. This also holds for different elements in the system: interactions will only matter if they occur in an element (levee section) which has a large influence on the system failure probability. The second factor depends on the degree of strength reduction, but also on the importance of the affected variable in the mechanism performance. In the conceptual examples, the strength was represented in only one variable which was weakened by the interaction. In reality, the strength is generally a combination of variables; if only one of those is weakened, the effect on the mechanism can be smaller.

To estimate the importance of interactions, a conventional reliability analysis (i.e. without interactions) can be used to map the (joint) reliability of all mechanisms and elements. This allows to identify critical elements and mechanisms. Secondly, it requires expert knowledge to identify which interactions are likely to occur and whether these interactions weaken critical mechanisms or elements.

5.2. Limitations of the quantification method

Here we discuss two limitations of the applied method, computational cost and time-dependent processes, for which other approaches (Section 2.3) may be more suitable.

First, the crude MCS method is computationally inefficient. In some cases, the effect of interactions can also be incorporated in a scenario-based approach using event trees, in combination with more efficient techniques such as FORM. For each failure path in the event tree that includes both the trigger mechanism and affected mechanism, the effect of the interaction is then incorporated by an adapted distribution of the affected variable. For this approach it is required that the sequence of events is known (or time is no variable at all) and that the effect of the interaction can be expressed as an adapted distribution of a variable $\hat{X}$. This requirement is met in the conceptual examples, and for the effect on uplift in levee example case 1, but not for the other levee cases and the effect on BEP through the changing seepage length.

For example, the failure probability of system 2 is the sum of the three failure path probabilities indicated by the black circles in the event tree in Fig. 12(a):

$$P_F = P(A \cap B) + P(A \cap \bar{B} \cap C \cap \hat{D}) + P(\bar{A} \cap C \cap D) \tag{20}$$

Here the overbar denotes non-occurrence, and $\hat{D}$ is mechanism D being evaluated with weakened $\hat{X}_5$ due to the interaction triggered by A. The individual event probabilities can be evaluated efficiently with FORM, and combined into path probabilities using their statistical correlation [16]. A similar approach can be followed for the levee example, as long as the aforementioned requirements are met (Fig. 12(b)).

When using simulation-based methods to evaluate the set of failure models, the efficiency can be improved using variance reduction techniques such as importance sampling, directional sampling and subset simulation. Applying FORM to the set of failure models may give convergence problems with the discontinuities introduced by the step function. This can be avoided by using continuous approximations of the step function.

The second limitation of the applied method is related to the time-dependence of failure processes within a flood event. When interaction does not only depend on the random variables in the same time step but also on previous time steps, it can become complicated to describe the failure model including interaction. For instance in the levee example the effect of interaction depends on previous time steps and not only on the current (e.g., Eqs. (12), (14) and (17)). Examples where this becomes more complicated are interactions driven by damages that accumulate each time step. In such cases it may become more practical to evaluate the limit states of each individual mechanism (so without step function describing the interaction) in two steps. After the first LSF evaluation, variables are updated based on the outcomes of the first LSF evaluation. Then, the mechanisms and system failure definition are re-evaluated using the updated variables. The updated variables are then taken to the next time step, which makes sure that the

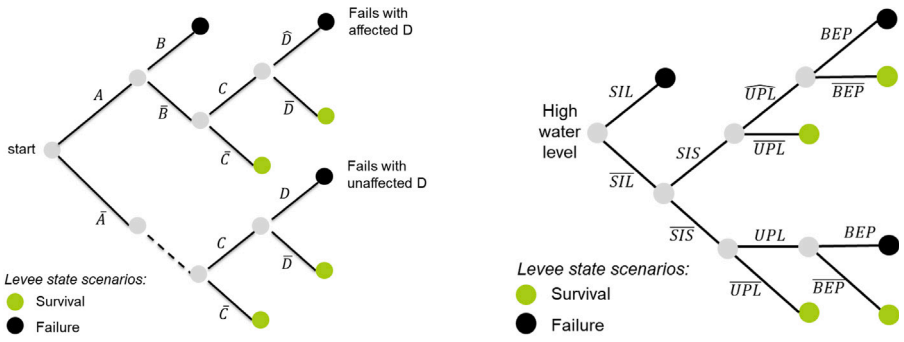

(a) Conceptual system 2 (b) Levee example

Fig. 12. Event trees of the conceptual example (a) and levee example (b). Branches represent (non-)occurrence of failure mechanisms: slope instability small (SIS) and large (SIL), blanket uplift (UPL) and backward erosion piping (BEP).

interaction effects propagate in time. For other examples such as interactions between transient groundwater flow and soil erosion, this approach cannot describe the processes and coupled modeling [36] may be more suitable. The levee example in this paper focuses on water level as driving load. Wind- and wave-driven failure processes also fit in the proposed method, but because these are more variable, the temporal correlation between those load variables should be considered in relation to the computational time step.

6. Conclusions

Physical interactions between failure mechanisms occur when a trigger mechanism changes physical properties of the system and thereby induce or prevent failure of other (affected) mechanisms. Unlike statistical correlation between mechanism performance, this type of dependence involves a physical change. We discussed different approaches to account for interactions in a reliability analysis, including coupled modeling of the physical processes and scenario-based reliability analysis using event trees. We applied an alternative quantification method based on Monte Carlo simulation. The interactions are included in the limit state functions using step functions. This allows for more flexibility compared to the scenario-based approach in event tree analyses. For instance, the analyst does not need to predefine the sequence in which mechanisms occur and affect other mechanisms. This method is applied to conceptual examples and to a levee subject to failure by landward slope instability and backward erosion piping. The conceptual examples show that the largest interaction effects are expected when the trigger mechanism is relatively likely and the affected mechanism has a relatively large contribution to the system reliability. The levee case study shows that minor slope instabilities which are too small to induce levee failure directly, can lead to levee failure by triggering another failure process (backward erosion through reduction of uplift resistance). In this case, the interaction increased the levee failure probability up to a factor 4. This interaction effect will be strongly case-dependent, for instance depending on the relative contribution of the trigger and affected mechanisms in the system reliability. Based on the findings from this research, further guidelines for practice can be developed that indicate under which conditions interactions need to be accounted for.

CRediT authorship contribution statement

Johannes C. Pol: Writing – original draft, Visualization, Methodology, Investigation, Conceptualization. **Paulina Kindermann:** Writing – review & editing, Software, Investigation. **Mark G. van der Krogt:** Writing – review & editing, Methodology. **Vera M. van Bergeijk:** Writing – review & editing, Methodology. **Guido Remmerswaal:** Writing – review & editing, Methodology. **Willem Kanning:** Writing – review & editing, Supervision, Methodology. **Sebastiaan N. Jonkman:** Writing – review & editing, Supervision. **Matthijs Kok:** Supervision, Funding acquisition.

Declaration of competing interest

The authors declare that they have no known competing financial interests or personal relationships that could have appeared to influence the work reported in this paper.

Data availability

Data will be made available on request.

Acknowledgment

This work is part of the Perspectief research programme All-Risk with project number P15-21D, which is (partly) financed by NWO Domain Applied and Engineering Sciences, Netherlands.

References

[1] Baecher GB, Christian JT. Reliability and statistics in geotechnical engineering. John Wiley Sons; 2005.
[2] Melchers RE, Beck AT. Structural reliability analysis and prediction. John Wiley Sons Ltd.; 2017.
[3] Jonkman SN, Kok M, Van Ledden MK, Vrijling JK. Risk?based design of flood defence systems: a preliminary analysis of the optimal protection level for the New Orleans metropolitan area. J. Flood Risk Manage. 2009;2(3):170–81.
[4] Vonk B, Klerk WJ, Fröhle P, Gersonius B, Den Heijer F, Jordan P, Radu Ciocan U, Rijke J, Sayers P, Ashley R. Adaptive asset management for flood protection: The FAIR framework in action. Infrastructures 2020;5(12):109.
[5] Steenbergen HMGM, Lassing B, Vrouwenvelder ACWM, Waarts PH. Reliability analysis of flood defence systems. Heron 2004;49(1):51–73.
[6] Morris MW, Allsop W, Buijs F, Kortenhaus A, Doorn N, Lesniewska D. Failure modes and mechanisms for flood defence structures. In: Samuels P, Huntington S, Allsop W, Harrop J, editors. FloodRisk2008. Oxford, UK: Taylor and Francis; 2008, p. 693–701.
[7] Kok M, Jongejan R, Nieuwjaar M, Tanczos I. Fundamentals of flood protection. The Hague, The Netherlands: Ministry of Infrastructure and the Environment and the Expertise Network for Flood Protection; 2017.
[8] Murthy DNP, Nguyen DG. Study of a multi-component system with failure interaction. European J Oper Res 1985;21(3):330–8.
[9] Sun Y, Ma L, Mathew J, Zhang S. An analytical model for interactive failures. Reliab Eng Syst Saf 2006;91(5):495–504.
[10] Meango TJM, Ouali MS. Failure interaction models for multicomponent systems: a comparative study. SN Appl. Sci. 2019;1(66).
[11] Lee Y-J, Song J. Risk analysis of fatigue-induced sequential failures by branch-and-bound method employing system reliability bounds. J Eng Mech 2011;137(12):807–21.
[12] Song J, Kang W-H, Lee Y-J, Chun J. Structural system reliability: Overview of theories and applications to optimization. ASCE-ASME J Risk Uncertain Eng Syst A 2021;7(2):03121001.
[13] Tazi N, Châtelet E, Bouzidi Y. How combined performance and propagation of failure dependencies affect the reliability of a MSS. Reliab Eng Syst Saf 2018;169:531–41.
[14] Zeng Z, Kang R, Chen Y. Using PoF models to predict system reliability considering failure collaboration. Chin J Aeronaut 2016;29(5):1294–301.

[15] Fang J, Kang R, Chen Y. Reliability evaluation of non-repairable systems with failure mechanism trigger effect. Reliab Eng Syst Saf 2021;210:107454.
[16] Roscoe K, Diermanse F, Vrouwenvelder T. System reliability with correlated components: Accuracy of the equivalent planes method. Struct Saf 2015;57(Supplement C):53–64.
[17] Jia G, Gardoni P. State-dependent stochastic models: A general stochastic framework for modeling deteriorating engineering systems considering multiple deterioration processes and their interactions. Struct Saf 2018;72:99–110.
[18] Meango TJ-M, Ouali M-S. Failure interaction model based on extreme shock and Markov processes. Reliab Eng Syst Saf 2020;197:106827.
[19] Murotsu Y, Okada H, Taguchi K, Grimmelt M, Yonezawa M. Automatic generation of stochastically dominant failure modes of frame structures. Struct Saf 1984;2(1):17–25.
[20] Karamchandani A, Dalane JI, Bjerager P. Systems reliability approach to fatigue of structures. J Struct Eng 1992;118(3):684–700.
[21] Andreini M, Gardoni P, Pagliara S, Sassu M. Probabilistic models for erosion parameters and reliability analysis of earth dams and levees. ASCE-ASME J Risk Uncertain Eng Syst A 2016;2(4):04016006.
[22] Adumene S, Khan F, Adedigba S, Zendehboudi S. Offshore system safety and reliability considering microbial influenced multiple failure modes and their interdependencies. Reliab Eng Syst Saf 2021;215:107862.
[23] Pei L, Chen C, He K, Lu X. System reliability of a gravity dam-foundation system using Bayesian networks. Reliab Eng Syst Saf 2022;218:108178.
[24] Wang Q, Jia G, Jia Y, Song W. A new approach for risk assessment of failure modes considering risk interaction and propagation effects. Reliab Eng Syst Saf 2021;216:108044.
[25] Van MA, Rosenbrand E, Tourment R, Smith P, Zwanenburg C. Failure paths for levees. Tech. rep., International Society of Soil mechanics and Geotechnical Engineering (ISSMGE) – Technical Committee TC201 'Geotechnical aspects of dikes and levees'; 2022.
[26] Calle EOF. Dijkdoorbraakprocessen. Tech. rep., GeoDelft; 2002.
[27] van der Krogt MG, Schweckendiek T, Kok M. Do all dike instabilities cause flooding? In: 13th international conference on applications of statistics and probability in civil engineering (ICASP13). 2019.
[28] USBR, USACE. Best practices in dam and levee safety risk analysis. Tech. rep., 2019.
[29] Remmerswaal G, Vardon PJ, Hicks MA. Evaluating residual dyke resistance using the random material point method. Comput Geotech 2021;133:104034.
[30] van Bergeijk VM, Verdonk VA, Warmink JJ, Hulscher SJMH. The cross-dike failure probability by wave overtopping over grass-covered and damaged dikes. Water 2021;13(5):690.
[31] CIRIA. The international levee handbook. London, UK: Ciria; 2013.
[32] Özer IE, van Damme M, Jonkman SN. Towards an international levee performance database (ILPD) and its use for macro-scale analysis of levee breaches and failures. Water 2020;12(1):119.
[33] Sills G, Vroman N, Wahl R, Schwanz N. Overview of new orleans levee failures: lessons learned and their impact on national levee design and assessment. J Geotech Geoenviron Eng 2008;134(5):556–65.
[34] Ubilla J, Abdoun T, Sasanakul I, Sharp M, Steedman S, Vanadit-Ellis W, Zimmie T. New orleans levee system performance during hurricane Katrina: London Avenue and Orleans canal south. J Geotech Geoenviron Eng 2008;134(5):668–80.
[35] Kanning W, Van Baars S, Vrijling JK. The stability of flood defenses on permeable soils: the London Avenue canal failures in New Orleans. 2008, p. 2.72.
[36] Rahimi M, Shafieezadeh A. Coupled backward erosion piping and slope instability performance model for levees. Transp. Geotechn. 2020;24:100394.
[37] Mizutani H, Nakagawa H, Yoden T, Kawaike K, Zhang H. Numerical modelling of river embankment failure due to overtopping flow considering infiltration effects. J Hydraul Res 2013;51(6):681–95.
[38] Fu Z, Su H, Han Z, Wen Z. Multiple failure modes-based practical calculation model on comprehensive risk for levee structure. Stoch. Environ. Res. Risk Assess. 2018;32(4):1051–64.
[39] Melchers RE, Beck AT. Time-dependent reliability. In: Structural reliability analysis and prediction. 2017, p. 179–245.
[40] Rubinstein RY, Kroese DP. Simulation and the monte carlo method. John Wiley and Sons; 2008.
[41] Hasofer AM, Lind NC. Exact and invariant second-moment code format. J. Eng. Mech. Divis. 1974;100(1):111–21.
[42] Dupuits EJC, Klerk WJ, Schweckendiek T, de Bruijn KM. Impact of including interdependencies between multiple riverine flood defences on the economically optimal flood safety levels. Reliab Eng Syst Saf 2019;191:106475.
[43] Phoon K-K. Numerical recipes for reliability analysis–a primer. In: Reliability-based design in geotechnical engineering. CRC Press; 2008, p. 13–87.
[44] Schweckendiek T, Vrouwenvelder ACWM, Calle EOF. Updating piping reliability with field performance observations. Struct Saf 2014;47:13–23.
[45] Tang C, Phoon KK. Model uncertainties in foundation design. CRC Press; 2021.
[46] Deltares. Modelonzekerheidsfactoren Spencer-Van der Meij model en ongedraineerde schuifsterkte. Deltares report 1207808-001. Tech. rep., Deltares; 2015.
[47] Geerse CPM. Hydra-Zoet for the fresh water systems in the Netherlands. Probabilistic model for the assessment of dike heights. Tech. rep. PR2168, HKV; 2011.
[48] Deltares. D-stability 20.1 user manual. Tech. rep., Deltares; 2019.
[49] Van M, Koelewijn AR, Barends F. Uplift phenomenon: Model, validation, and design. Int J Geomech 2005;5(2):98–106.
[50] Ladd CC, Foott R. New design procedure for stability of soft clays. J. Geotechn. Eng. Divis. 1974;100(7):763–86.
[51] Sudret B. Meta-models for structural reliability and uncertainty quantification. In: Asian-pacific symposium on structural reliability and its applications. Research Publishing; 2012, p. 1–24.
[52] Li D-Q, Zheng D, Cao Z-J, Tang X-S, Phoon K-K. Response surface methods for slope reliability analysis: Review and comparison. Eng Geol 2016;203:3–14.
[53] USACE. Design and construction of levees. engineer manual. Tech. Rep. EM 1110-2-1913, 2000.
[54] TAW. Technisch rapport waterspanningen bij dijken. Tech. Rep. DWW-2004-057, 2004.
[55] Sellmeijer H, de la Cruz JL, van Beek VM, Knoeff H. Fine-tuning of the backward erosion piping model through small-scale, medium-scale and Ijkdijk experiments. Eur J Environ Civ Eng 2011;15(8):1139–54.